An Observationally-Based Evaluation of Sub-Grid Scale Ice Thickness Distributions Simulated in a Large-Scale Sea Ice - Ocean Model of the Arctic Ocean

Mischa Ungermann[1], Martin Losch[1]

[1]Alfred Wegener Institute, Helmholtz Centre for Polar and Marine Research, Bremerhaven, Germany

Key Points:

- Recent observations allow to evaluate ice thickness distributions in the Arctic on regional to local scales.
- A pan-Arctic model simulates the observed regional and seasonal range of ice thickness distributions with some skill.
- The model underestimates the decadal variability of ice thickness distributions.

Corresponding author: Martin Losch, `martin.losch@awi.de`

Abstract

A key parameterization in sea ice models describes the sub-grid scale ice thickness distribution. Based on only a few observations, the ice thickness distribution model was shown to be consistent with field data and to improve the simulation's large scale properties. The available submarine and airborne observations enable to evaluate in greater detail the ability of a pan-Arctic sea ice - ocean model with an ice thickness distribution parameterization to reproduce observed thickness distributions in different regions and seasons. Many observations are reproduced accurately. Some cases of poorly simulated modes and tails of the distributions are tentatively attributed to simplified thermodynamics and inaccurate deformation fields. Variability on decadal timescales, however, is generally underestimated. Thickness distributions in individual grid cells of the model show similar differences between regions and seasons as observed regional mean distributions, but the modeled grid-scale variability is lower than observed. Simulated modal thicknesses of first-year ice are only insufficiently different from those of multi-year ice. The modal thickness proves to be a useful metric for quantifying model biases in both dynamics and thermodynamics. In addition to improving basin-wide mean variables, the ice thickness distribution parameterization provides reliable and valuable additional sub-grid scale data. At the same time the low climate sensitivity of the parameterization may affect longer simulations with strong climate change aspects.

1 Introduction

The Arctic is changing rapidly. Especially the ice cover is in a transition from a perennial to a seasonal state [*Overland et al.*, 2013]. In this situation, evaluating and improving the physical basis of sea ice models becomes increasingly important: (1) climate predictions depend on sea ice models to realistically represent both the feedback processes in the Arctic and the connections between Arctic phenomena and lower latitudes [*Hunke et al.*, 2010]. (2) The reduced sea ice cover sparks economic interest in marine operations like shipping or offshore exploration. Ensuring their safety requires reliable information about the ice cover [*Arctic Council*, 2009].

In this context, small openings in the ice pack, starting from small cracks up to larger leads between floes or linear kinematic features in the ice more than 100 km long, appear as important features whose effect needs to be included in sea ice models. The thin ice in these openings allows for a heat exchange between ocean and atmosphere that is larger by one to two orders of magnitude than the heat exchange over perennial ice [*Maykut*, 1978]. For shipping in an ice covered ocean, leads mark divergent regions in the ice pack and often prescribe the most efficient or only possible routes. These sub-grid scale features are not wide enough to be fully resolved even in very-high resolution sea ice models [*Hutter et al.*, 2018] and need to be parameterized.

In addition to small openings in the ice, the ice thickness itself varies at the horizontal meter scale. These thickness variations are important for sea ice models, because the ice growth rate depends inversely, hence non-linearly on ice thickness. Since it is impossible to resolve these variations directly, a sub-grid scale Ice Thickness Distribution (ITD) parameterization was a key element in the first sea ice models [*Coon et al.*, 1974; *Thorndike et al.*, 1975]. This model component has been adopted in many current climate models [*Stroeve et al.*, 2014] and has been shown to improve the representation of sea ice in in numerical models [*Holland et al.*, 2006; *Massonnet et al.*, 2011; *Komuro and Suzuki*, 2013; *Ungermann et al.*, 2017]. Further, an ITD model made possible additional sophisticated parameterizations, for example, a melt pond parameterization [*Flocco and Feltham*, 2007], or a refined surface stress parameterization [*Tsamados et al.*, 2014].

Although this parameterization has been widely used, it was not possible until recently to evaluate the simulated ITDs comprehensively, because not enough reliable observations were available. Simulated ice thickness distributions in individual grid cells of early Arctic ITD-enabled models were compared to ice thickness observations from submarines [*Hibler*, 1980; *Flato and Hibler*, 1995]. The results were mixed, because only very few data points were available for comparison and there were large differences between these individual measurements. Submarine thickness observations were also found to be too sparse to properly constrain a fully coupled climate model [*Bitz et al.*, 2001], so that, in extension of the model-observation comparison, the authors focused mostly on changes between model configurations with and without the ITD parameterization. More recent evaluations of Arctic ocean sea ice models often used large sets of different observations to assess the model including observed ITDs, for example, from moorings [*Dupont et al.*, 2015] or airborne sounding [*Herzfeld et al.*, 2015]. After averaging over multiple years [*Dupont et al.*, 2015] or over a large region [*Herzfeld et al.*, 2015], the models simulated the observed ITDs accurately.

The ITD parameterization has been tested in a Lagrangian sense without being embedded in a dynamic-thermodynamic sea ice model, but forced by observed deformation and energetic fields. An ITD model of the immediate environment of the drift camp of the Surface Heat Budget of the Arctic Ocean (SHEBA) experiment was initialized and forced by sea ice deformation, atmosphere– and ocean state from direct observations, but the evaluation suffered from the fact that there were no thickness observations beyond the initialization phase [*Lindsay*, 2003]. A coastal draft distribution model, forced with high-precision meteorological observations obtained at the coast, was found to be largely consistent with draft observations from moorings, but produced excessive ridging [*Bellchamber-Amundrud et al.*, 2002]. A new redistribution model very accurately simulated observed ice thickness distributions from high-resolution field data in the Gulf of St. Lawrence, but the simulation and observation period covered only individual strong deformation events (a storm) over a few days [*Kubat et al.*, 2010].

In summary, different ITD models have been shown to reproduce different observations of Arctic ITDs. But at the same time, most authors note that the model results do not match observations in the generation of open water, or in the amount of very thick ice produced by ridging, or in the amount of ridging in shearing motion. The most important processes that form ITDs locally are different in different regions of the Arctic and may require individual tuning to the local environment. Resulting biases can be reduced based on individual local observations. Still it is unclear if a pan-Arctic sea ice model that uses one ITD parameterization with a globally fixed set of parameters can describe different sea ice regimes accurately.

The number of high-resolution sea ice thickness observations has grown steadily over the past decades. New Airborne ElectroMagnetic (EM) sounding of ice thickness [*Haas et al.*, 2010] complement the Upward-Looking Sonar (ULS) measurements from submarine cruises [*Rothrock and Wensnahan*, 2007], and detailed evaluations of ice thickness distributions become finally possible. We use this much larger, and until recently unavailable, database and investigate the extent to which ITD parameterizations can reproduce regional, seasonal and decadal variability in Arctic ITDs. In the evaluation of the model results, we focus on three aspects: (1) Does the model reproduce regional averages of observed distributions? (2) Does the model reproduce single observations at the grid scale? And (3) which mechanisms and model parameters have the highest impact on the modeled ITDs? The data set we use and a description of the ITD model are presented in section 2. Model – observation comparisons and the results of additional sensitivity studies are presented in section 3. These results are discussed in section 4, and the main conclusions are drawn in section 5.

2 Methods

2.1 Observations

Since 1958, submarines sailing under the Arctic sea ice have been equipped with Upward-Looking Sonar (ULS) that measure the draft of the sea ice. A recent collection of submarine-based ULS data and draft distributions for 50km segments of submarine tracks covers a large part of the Arctic Ocean and spans the years 1975 to 2005 [*Lindsay and Schweiger*, 2013]. Airborne electromagnetic (EM) sounding measurements of combined ice and snow thickness [e.g. *Haas et al.*, 2008, 2010] complement this ULS data set of the last 15 years. The lengths of the individual flight tracks during those campaigns differ, but they are also in the order of 50km. In this study, we select a subset of these observations in four regions (1) Beaufort Sea, (2) Lincoln Sea, (3) Fram Strait and (4) Central Arctic (Figure 1). In each of these regions measurement campaigns collected data in similar periods of multiple years, so that we can calculate regional mean thickness distributions. Note that these averages may not be representative of actual sea ice conditions. It is possible that distributions are calculated from the ensemble of observations of extremely different ice conditions in different years. Nevertheless, these distributions over a larger sample size of comparable forcing conditions allow to test model performance without the need to reproduce individual weather events. The sampled observations cover different seasons and different decades. The ULS data selected for this study are from the years 1986 – 1997 and the EM data are from the years 2001 – 2012. Table 1 summarizes the exact years and seasons of the observational data sets.

ULS and EM soundings can determine the thickness of undeformed ice with high accuracy, but they have known biases for ridged ice. The ULS data tend to overestimate the thickness by 29 cm ± 25 cm [*Rothrock and Wensnahan*, 2007]. One important source of error is that the sensors record the fastest reflection of the emitted acoustic signal, so that instead of the mean draft, the maximal draft over the footprint of the sensor is observed. Especially for rough, strongly deformed ice, this leads to an overestimated ice draft. The uncertainties in the EM data are as low as 10 cm for level ice [*Pfaffling et al.*,

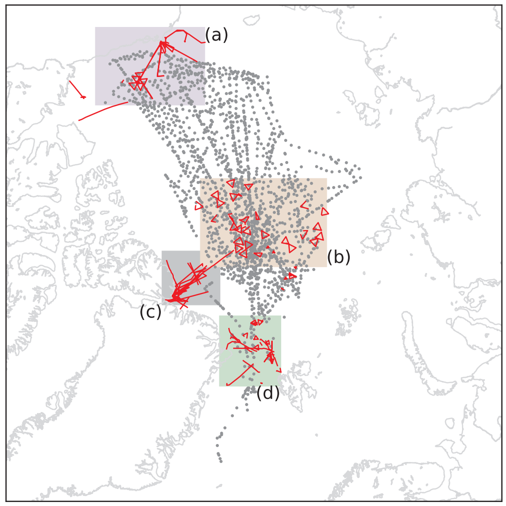

Figure 1. Overview of available observations: orange lines for EM-Bird flights, gray dots for ULS submarine track segments. Shaded areas are the model regions for comparison in (a) Beaufort Sea, (b) Central Arctic, (c) Lincoln Sea, (d) Fram Strait.

2007], but again the thickness of deformed ice is less accurate. In contrast to the ULS data, the electromagnetic sounding measures a weighted mean over a large footprint, so that the thickness of individual ridges is mostly smoothed out by the surrounding thinner ice. Hence, in EM data the thickness of ridges, and consequently the tail of thickness distributions, is underestimated [*Reid et al.*, 2006]. The obtained mean ice thickness is too low in the presence of ridges, but the size of this bias is difficult to estimate. The footprint of the sensors is between 2.6 m and 6 m for ULS data [*Rothrock and Wensnahan*, 2007] and about 45 m to 75 m for EM data [*Reid et al.*, 2006; *Johnston and Haas*, 2011].

When comparing ULS and EM observations to each other, we convert the ice draft to combined ice and snow thickness using the time-dependent values for snow thickness and snow density of *Warren et al.* [1999] and constant values $\rho_w = 1027 \mathrm{kg/m^3}$ and $\rho_i = 928 \mathrm{kg/m^3}$ for the densities of water and ice [*Rothrock et al.*, 2008]. To visualize ITDs, we plot the probability density for both observations and model data. This allows for a direct visual comparison of results, even when the bin sizes of the model are variable. Finally, with both measurement techniques it is difficult to distinguish thin ice from open water. For this reason, areas with open water are excluded from the calculation of ITDs in this study.

Table 1. Overview of observational data sets

	region[1]	years	months	source	# obs[2]	# campaigns[3]
(S1)	Beaufort Sea	1986–1994	Apr	ULS	32	6
(S2)	Beaufort Sea	1993–1997	Sep, Oct	ULS	54	4
(S3)	Central Arctic	1989–1997	Sep	ULS	117	6
(S4)	Central Arctic	1986–1994	Apr, May	ULS	202	14
(S5)	Fram Strait	1987–1991	Apr, May	ULS	42	2
(S6)	Beaufort Sea	2007–2011	Apr	EM	25	7
(S7)	Lincoln Sea	2004–2012	Apr, May	EM	30	9
(S8)	Central Arctic	2001–2011	Aug, Sep	EM	37	3
(S9)	Fram Strait	2004–2011	Aug	EM	15	3
(S10)	Fram Strait	2003-2011	Apr, May	EM	12	4

[1] Regions as defined in Figure 1

[2] submarine track segments / individual EM-flights

[3] submarine cruises / EM measurement campaigns

2.2 Model Equations

We use the Massachusetts Institute of Technology general circulation model (MITgcm, version checkpoint 66a) [*Marshall et al.*, 1997; *MITgcm Group*, 2016] for our numerical experiments. The model region is the northern cap of a cubed-sphere geometry with an average grid resolution of 36km and boundaries at roughly 55° north in both the Atlantic and the Pacific Ocean [*Nguyen et al.*, 2011]. The necessary boundary conditions are taken from the Estimating the Circulation and Climate of the Ocean, Phase II project (ECCO2) [*Menemenlis et al.*, 2008]. The NCEP Climate Forecast System Reanalysis is used as atmospheric forcing [*Saha et al.*, 2010]. The sea ice component of the MITgcm [*Losch et al.*, 2010] includes dynamics, zero-layer thermodynamics and a dynamic ITD model following *Thorndike et al.* [1975] and *Lipscomb et al.* [2007].

2.2.1 Sea Ice Dynamics

The vector $\boldsymbol{u}$ of sea ice velocity is calculated according to the momentum balance

$$m\frac{\partial \boldsymbol{u}}{\partial t} = -mf_C\boldsymbol{k}\times\boldsymbol{u} + \boldsymbol{\tau_a} + \boldsymbol{\tau_o} - m\hat{g}\Delta_H + \nabla\cdot\boldsymbol{\sigma}, \tag{1}$$

where $m = \rho_i H_i + \rho_s H_s$ is the ice and snow mass per unit area, calculated from the respective densities ρ_i, ρ_s and grid cell area averaged thicknesses H_i, H_s of ice and snow. The forcing terms on the right hand side of (1) are: the horizontal Coriolis force with the Coriolis parameter f_C and the vertical unit vector $\boldsymbol{k}$; the interfacial stress between atmosphere and ice $\boldsymbol{\tau_a}$ and ocean and ice $\boldsymbol{\tau_o}$; the sea surface tilt Δ_H with the gravitational acceleration $\hat{g}$; and the divergence of the internal ice stress tensor $\boldsymbol{\sigma}$. The stresses from atmosphere and ocean on the ice are calculated using the quadratic laws

$$\boldsymbol{\tau_a} = \rho_a c_{d,a}|\boldsymbol{u_a} - \boldsymbol{u}|\boldsymbol{R_a}(\boldsymbol{u_a} - \boldsymbol{u}) \tag{2}$$

$$\boldsymbol{\tau_o} = \rho_o c_{d,o}|\boldsymbol{u_o} - \boldsymbol{u}|\boldsymbol{R_o}(\boldsymbol{u_o} - \boldsymbol{u}) \tag{3}$$

where ρ_a and ρ_o are the reference densities, $c_{d,a}$ and $c_{d,o}$ the drag coefficients, $\boldsymbol{u_a}$ and $\boldsymbol{u_o}$ the velocities, and $\boldsymbol{R_a}$ and $\boldsymbol{R_o}$ rotation matrices for the atmosphere (subscript a) and ocean (subscript o) [*McPhee*, 1975]. More sophisticated parameterizations of drag and drag coefficients in terms of roughness length are available [*Tsamados et al.*, 2014; *Roy et al.*, 2015], that better reflect the complexity of the processes in drag, but for simplicity we employ a commonly used constant drag coefficients formulation. Advection of momentum is neglected in the momentum balance (1), and for simplicity we set the rotation matrices $\boldsymbol{R_a}$, $\boldsymbol{R_o}$ in equations (2) and (3) to unity.

Closing the momentum balance (1) requires a relationship between the stress tensor and the ice drift velocities. We use the standard Reiner-Rivlin constitutive relation for a viscous-plastic rheology [*Hibler*, 1979] that relates the internal ice stress $\boldsymbol{\sigma}$ to the strain rate $\dot{\boldsymbol{\varepsilon}} = \frac{1}{2}\left[\nabla\boldsymbol{u} + (\nabla\boldsymbol{u})^T\right]$:

$$\boldsymbol{\sigma} = 2\eta\,\dot{\boldsymbol{\varepsilon}} + \left([\zeta - \eta]\,\dot{\varepsilon}_I - \frac{P}{2}\right)\boldsymbol{I}. \tag{4}$$

Here the bulk viscosity $\zeta = \frac{P}{2\Delta_{\dot{\varepsilon}}}$ and the shear viscosity $\eta = \frac{\zeta}{e^2}$ are calculated from the ice pressure P, the axis ratio e of the elliptical yield curve, and the strain rate tensor $\dot{\boldsymbol{\varepsilon}}$ invariants, that is, divergence $\dot{\varepsilon}_I = \dot{\varepsilon}_{11} + \dot{\varepsilon}_{22}$ and shear $\dot{\varepsilon}_{II} = \sqrt{(\dot{\varepsilon}_{11} - \dot{\varepsilon}_{22})^2 + 4\dot{\varepsilon}_{12}^2}$. $\boldsymbol{I}$ is the identity matrix and $\Delta_{\dot{\varepsilon}} = \sqrt{\dot{\varepsilon}_I^2 + e^{-2}\dot{\varepsilon}_{II}^2}$ is a convenient measure of deformation specific to the elliptical yield curve. The compressive strength is related to the ice thickness h and sea ice fractional area A [*Hibler*, 1979] through:

$$P = P^* A h e^{-C^*(1-A)}. \tag{5}$$

We briefly introduce three parameterizations of sub-grid scale processes whose impact on modeled ITDs will be investigated later: (1) a gross closing rate R_c of the ice pack is calculated as

$$R_c = \text{convergence} + C_s * \text{shear} \tag{6}$$

where convergence $= -\min(\dot{\epsilon}_I, 0)$ and shear $= \frac{1}{2}(\Delta_{\dot{\epsilon}} - \text{abs}(\dot{\epsilon}_I))$. The factor $0 \leq C_s \leq 1$ determines how much of the shearing motion of the ice pack can be translated to a closing motion of differently aligned leads, which then ridges ice after the lead is closed [*Flato and Hibler*, 1995]. (2) A lead closing parameter H_0 determines how much of newly formed ice volume is distributed laterally in open water [*Hibler*, 1979]. The lead closing parameterization was introduced in 2-category models [*Hibler*, 1979] to efficiently summarize many small-scale processes during ice formation. With a smaller value, open water freezes more quickly and inhibits further heat flux. With a larger value of H_0, leads stay open longer which eventually leads to more ice volume in the simulation. In our ITD model, we apply this parameterization only to the thinnest ice category. This treatment of new ice is slightly different to other ITD-enabled models [e.g., *Lipscomb et al.*, 2007], where new ice fills the thinnest category uniformly first and then is ridged into thicker categories. And (3) during ridging, a fraction of snow $(1 - F_S)$ with $0 \leq F_S \leq 1$ is pushed into the water [*Flato and Hibler*, 1995].

2.2.2 Ice Thickness Distribution

The thickness distribution $g(h)$ describes the relative amount of ice with thicknesses between h and $h + dh$ [*Thorndike et al.*, 1975]. This distribution can change by advection, thermodynamics or through ridging. In our simulations, the mechanical changes due to ridging are parameterized following *Thorndike et al.* [1975] and *Lipscomb et al.* [2007]. In this theory, the horizontal ice motion determines how much ice ridges due to convergence and shear. When ridging takes place, ice with the distribution $a(h)$ deforms. This distribution consists mostly of the available thin ice. Ice of initial thickness h_{in} is ridged into a distribution $\gamma(h_{\text{in}}, h)$, so that the new ice created by ridging has the thickness distribution

$$n(h) = \int_0^{h_{\max}} a(h_{\text{in}})\gamma(h_{\text{in}}, h)\, \mathrm{d}h_{\text{in}} \tag{7}$$

for an initial ice cover with a maximal thickness $h_{\max}$.

We use smooth and differentiable participation and redistribution functions [*Lipscomb et al.*, 2007]. The participation function

$$a(h) = \frac{1}{b_0} \exp\left(\frac{-G(h)}{a^*}\right) g(h) \tag{8}$$

determines how much of the ice of thickness h takes part in each ridging event. b_0 is a normalization factor, $G(h) = \int_0^h g(\hat{h})\, \mathrm{d}\hat{h}$ is the cumulative thickness distribution and a^* is the participation parameter that scales the relative participation of thin and thick ice. And the redistribution function

$$\gamma(h_{\mathrm{in}}, h) = \gamma_0 \exp\left(\frac{-(h - h_{\min})}{\mu\sqrt{h_{\mathrm{in}}}}\right) \tag{9}$$

describes how much ice is ridged into thickness h with each ridged unit area of ice of thickness h_{in}. γ_0 is a normalization factor, μ is a scaling parameter, and $h_{\min} = h_{\min}(h_{\mathrm{in}})$ is the minimal thickness into which ice of thickness h_{in} can be ridged.

2.2.3 Sensitivity Analysis

Sensitivities of the simulated ITDs to ten different parameters are inferred from the differences between a positive and a negative perturbation run for each parameter. As a measure of distance between two histograms, we calculate the area between the cumulative thickness distributions

$$d_{\mathrm{hist}}(g_1, g_2) = \int_0^{h_{\max}} |G_1(h) - G_2(h)|\, \mathrm{d}h, \tag{10}$$

so that a larger area denotes larger differences between the distributions. This measure is known as the ”Earth mover’s Distance“: for piles of earth (hence the name), this measure calculates the minimal amount of work that is necessary to transform one distribution into the other [*Rubner et al.*, 2000]. With this measure, histograms in different bins can easily be compared and cross-bin similarities are taken into account.

Sensitivities of the simulated ITDs to ten different parameters are inferred from perturbation runs. For each parameter, two simulations are performed with a positive and a negative perturbation; the parameter ranges are given in Table 2. For the mean ITDs in the regions defined in Table 1 and Figure 1, the mean difference d_{hist} between the ITDs from the two perturbed simulations is used to indicate the sensitivity of the modeled ITDs to this parameter.

Table 2. Parameter values in sensitivity analyzes and final configuration

	Description	Baseline	Perturbation Range	Final
μ ($m^{\frac{1}{2}}$)	redistribution	3.029	2.029 – 4.029	2.0
a^*	participation	0.041	0.031 – 0.051	0.03
P^* ($kN\,m^{-2}$)	ice strength	22.99	20.0 – 27.0	22.0
C^*	strength parameter	15.92	12.0 – 20.0	10.0
$c_{d,a} \times 10^3$	atmospheric drag	1.657	1.4 – 1.9	1.9
$c_{d,o} \times 10^3$	oceanic drag	6.647	6.147 – 7.147	6.5
e	axis ratio of ellipse	1.523	1.123 – 1.923	1.8
C_s	ridging in shear	0.5	0.25 – 0.75	0.85
H_0 (m)	ice growth	0.565	0.415 – 0.715	0.6
F_s	snow fraction in ridging	0.5	0.25 – 0.75	0.6

The tested parameters are listed in Table 2. They are: the two redistribution parameters (1) a^*, that determines which ice takes part in ridging processes and (2) μ, that determines the shape of the produced ridges; (3) the compressive ice strength parameter P^* and (4) the ice concentration parameter C^*, of the ice strength parameterization; the drag coefficients (5) $c_{d,a}$ and (6) $c_{d,o}$ for the ice with respect to atmosphere and ocean; (7) the axis ratio e of the elliptical yield curve, which determines the ratio between shear strength and compressive strength P in the VP-rheology; (8) the shear coefficient C_s, which determines how much energy is used to build pressure ridges in shear deformation; (9) the lead closing parameter H_0; and (10) the snow fraction F_s that remains on the ice after ridging.

2.3 Model Data

An Arctic configuration of the MITgcm is compared against the observational data. The model setup in this study is based on previous Arctic configurations using the ITD parameterization and the Hibler-type strength (5) [*Ungermann et al.*, 2017]. The ITD is discretized into ten thickness categories with the bounds 0.0m, 0.32m, 0.66m, 1.04m, 1.47m, 2.01m, 2.74m, 3.78m, 5.36m, 7.74m. This configuration was chosen as a compromise between computational costs and sufficient thickness resolution. The sensitivity analysis informed a manual adjustment of the parameters. The final values, which were chosen so that they improve the representation of the ITD in the model without departing too far from the mean sea ice state of the configurations in *Ungermann et al.* [2017], are also summarized in Table 2. After a five-year spinup with periodic forcing, the model is integrated over the years 1979 to 2011.

Model results are compared to observations of either ice draft (ULS) or combined ice and snow thickness (EM). In the MITgcm, the ice draft

$$h_d = \frac{\rho_i h_i + \rho_s h_s}{\rho_w} \tag{11}$$

and the total ice and snow thickness

$$h_t = h_i + h_s \tag{12}$$

can be calculated from the thicknesses h_i, h_s and densities ρ_i, ρ_s of ice and snow (subscripts i and s) and the surface density ρ_w of the ocean.

The data coverage allows to assess both regionally averaged ITDs and individual measurements. The modeled thickness distributions are averaged over the regions and months of the year defined in Table 1 to be compared to the corresponding averages of the observations. Track segments of the ULS data and individual flights of the EM data are compared to ten-day model snapshots. Each data set is associated with the nearest grid cell and the appropriate ten-day snapshot.

3 Results

3.1 Modeled Sea Ice Climate

A quadratic cost function measures the overall performance of our model configuration. The difference between model results and satellite observations is calculated for each point, weighted by the individual measurement uncertainties, and then the squared weighted differences are summed. This quantitative indicator of model quality can be computed for each satellite product. For more details, the reader is referred to *Ungermann et al.* [2017]. In our case, the differences to satellite observations of sea ice concentration [*EUMETSAT Ocean and Sea Ice Satellite Application Facility*, 2011], sea ice thickness [*Kwok and Cunningham*, 2008] and sea ice drift during winter and summer months [*Lavergne et al.*, 2010; *Kimura et al.*, 2013] weighted by measurement uncertainties are evaluated in this way. For ice concentration the uncertainties are provided with the data, for ice thickness they are taken as the minimum of 40% of the data value and 1 m, and for ice drift they are constructed from comparisons of different drift data sets [*Sumata et al.*, 2014, 2015]. The cost function contribution is normalized by the number of individual observations for each satellite separately, so that variables with different numbers of data points have the same weight in the total cost function (the sum of all contributions). The contribution of an individual satellite product is one when the average of the model-data misfit in each point is as large as the corresponding measurement uncertainty. In addition, the sum of the distances d_{hist} between model results and observations for the ten regions defined in Table 1 is calculated as a measure of the overall quality of the modeled ITDs.

The cost function terms and the quantitative ITD comparisons are summarized in Table 3 for the configuration used in this study and two configurations from *Ungermann et al.* [2017]: the best configuration of the latter study "ITD5H" with with five thickness categories and a Hibler-type ice strength parameterization and a reference configuration "noITD" without an dynamic ITD parameterization. This comparison is not completely unbiased, because the measure d_{hist} depends slightly on the resolution of the ITD, and because the ITDs for the configuration "noITD" are calculated from mean thickness per grid cell in the respective regions only. Still, the combination of the results shows that the tuning described in Section 2.2.3 permits a better representation of the ITDs. These improvements are mainly obtained in the comparisons with the EM data. Some Arctic-wide sea ice features, such as concentration and winter drift, cannot be improved by tuning the model to ITD, and their cost function contributions increase. The overall model quality with the adjusted parameters as measured by the cost function, however, is comparable to a well-tuned configuration without an active ITD.

In addition, we compare model results for Arctic-wide sea ice volume and extent to the results from the Pan-Arctic Ice Ocean Modeling and Assimilation System [PIOMAS, *Schweiger et al.*, 2011] and to observations from the Sea Ice Index [*Windnagel et al.*, 2016] in Figure 2. For both variables the model simulates a seasonal cycle with the same timing as in the reference data, but a slightly lower magnitude. Note that the model does not show the unrealistically high seasonality that is expected of models using 0-layer thermodynamics [*Semtner*, 1984]. The model tends to underestimate the sea ice volume and at the same time overestimate the extent, indicating that the modeled mean ice thickness is too low. For both variables, the linear trend over the three decades is clearly lower in the model than in the reference data, independent of the different signs in model bias. The year-to-year variability in the observations is captured for extent, but for volume there are

Table 3. Cost Function Values and d_{hist} for Regional ITDs

	present study	ITD5H (2017)[1]	noITD (2017)[2]
concentration	1.75	1.57	1.69
thickness	0.63	0.63	0.75
winter drift	0.65	0.45	0.5
summer drift	0.9	0.95	1.03
Total cost function	**3.94**	**3.59**	**3.97**
d_{hist} EM	2.92	4.19	4.26
d_{hist} ULS	5.26	5.54	7.15
Total d_{hist}	**8.18**	**9.73**	**11.41**

[1] ITD with 5 categories + Hibler-type strength [*Ungermann et al.*, 2017]

[2] Two-category thickness model [*Ungermann et al.*, 2017]

larger differences between consecutive years in the PIOMAS model than in our MITgcm simulation.

3.2 Regional Ice Thickness Distributions

We first compare the model simulation to the ten data sets of Table 1 (Figure 3).

Similar to the observations, the modeled ice thickness distributions vary between regions, but there are differences in the accuracy of the modeled ice conditions that appear to depend on the ice type. In predominantly first-year ice in the Beaufort Sea and in the Central Arctic during the 2000s, the agreement between model and observations is very high (Figure 3, (S1), (S2), (S6), and (S8)). For example, the integrated differences d_{hist} between the cumulative histograms of observations and model distributions of 0.33m, 0.43m and 0.47m are much lower in the Beaufort Sea than the average over all regions of 0.64m ± 0.21m. In regions with more multi-year ice, the model still captures the overall properties of the ice pack, but especially for bi-modal distributions (Figure 3, (S3), (S9), and (S10)), the agreement with the observed ITDs is lower. The seasonal variations in the ITDs are also best represented with first-year ice: The model slightly underestimates the changes in the Beaufort Sea (S1 vs. S2), while it strongly overestimates the annual cycle in the Central Arctic (S3 vs. S4) and in the Fram Strait (S9 vs. S10).

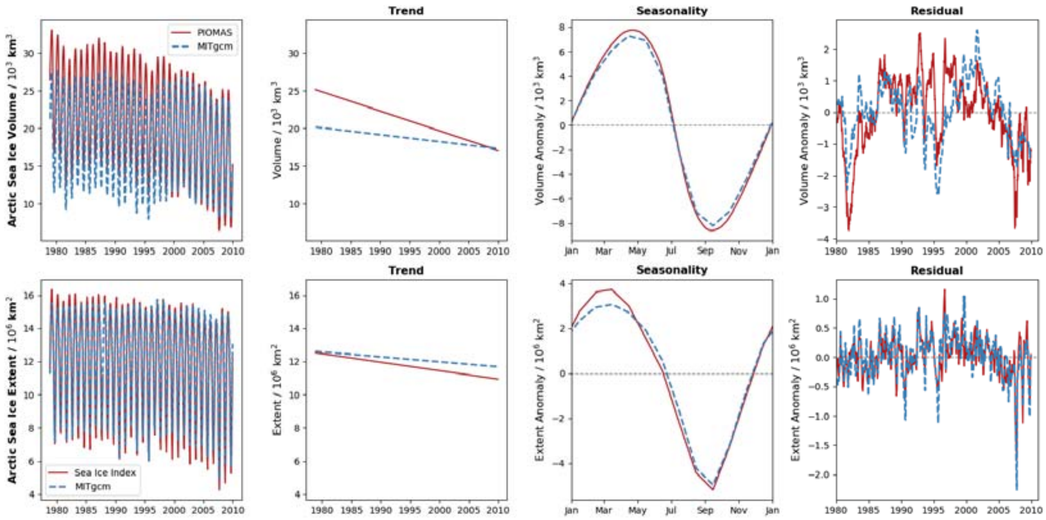

Figure 2. Comparison of the MITgcm against PIOMAS (Arctic Sea Ice Volume) and the Sea Ice Index (Arctic Sea Ice Extent). The time series are separated into a linear trend, a seasonal fluctuation and the residual that is not explained by the two.

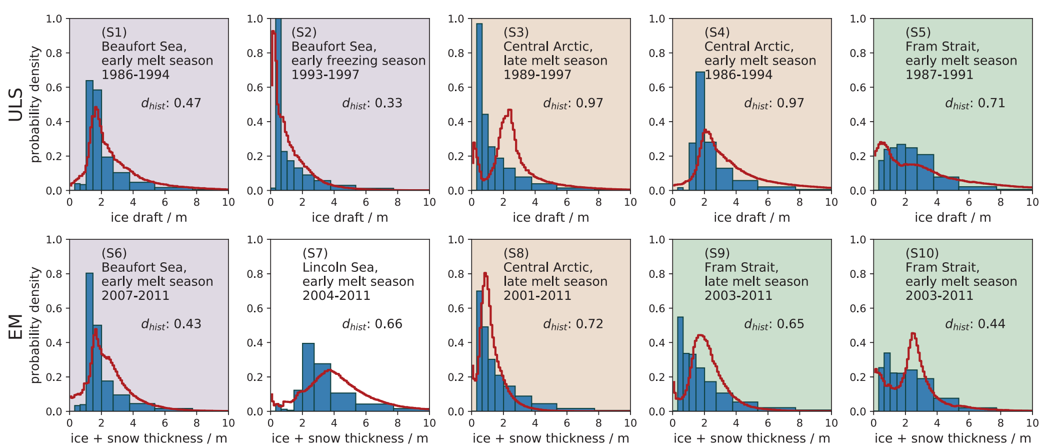

Figure 3. Regional ITDs from model (blue bars) and observations (red line). Observations are ice draft from submarine ULS (S1)–(S5), ice + snow thickness from airborne EM sounding (S6) – (S10). Exact regions and times of comparisons are specified in Figure 1 and Table 1.

The model does not simulate large decadal differences in ITDs. We compare average distributions of combined model ice and snow thickness centered at 1990 and 2005 for regions and seasons in analogy to the observations S1, S2, S3, S4, S5, S7 and S9 (see Table 1). On average, the modal thicknesses of the model distributions do not change over these years (0m ± 0.02m). In this evaluation, S5 is excluded because the distribution is very flat around its mode. Over the same time, the mean thicknesses of the modeled distributions decrease only by 0.06m ± 0.12m. In comparison, for the three regions with observations in different decades, the estimated loss in mean ice and snow thickness is 0.88m (S1 and S6, Beaufort Sea), 1.79m (S3 and S8, Central Arctic) and 1.37m (S5 and S10, Fram Strait).

The model underestimates both modal and mean thickness compared to observations, but the differences are smaller for the mean than for the mode. On average, the modal thicknesses of the ten regions are thinner by 0.66m ± 0.89m in the model than in the observations, while the difference for the mean thicknesses is only 0.25m ± 0.47m, indicating that the distributions in the model are skewed compared to the observations: While the mode in the model is often unrealistically thin and introduces too much thin ice into the distribution, its effect on the mean thickness is partially offset by too much ridged ice and too little ice that is thinner than the mode.

The exponential tails in the distributions further illustrate these differences in the shape of the ITDs. Both the observed and the modeled ITDs show an exponential tail, but the rate parameters (or the slopes in the semi-logarithmic plot) are different (Figure 4). While the qualitative behavior of the tail agrees between model and observations, the rate parameter of the modeled tail differs in most regions from the observations. Of the three regions in Figure 4, the distribution tails of model and observations agree in the Beaufort Sea mostly because the observed distribution is very different from other regions. The thickness distributions in Figure 4 were chosen to represent the range of distribution tails in the model and the observations. In other regions the distributions decay with comparable exponential tails.

3.3 Grid-Scale Ice Thickness Distributions

Draft distributions from five different submarine track segments are compared to the distributions taken from the nearest model grid cell (Figure 5). We note, that this comparison is more sensitive to biases in the ITD parameterizations than the comparison of

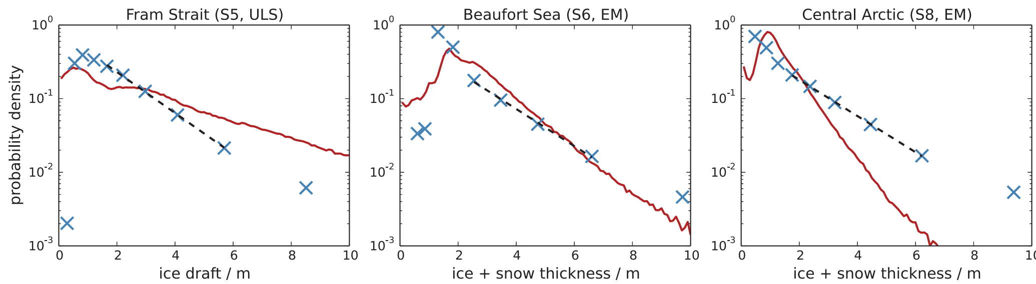

Figure 4. Semi-logarithmic plot of average ice draft h_d or ice and snow thickness h_t against probability density in each category for three regional ITD. Blue crosses for model values, red lines for observations. The dashed black lines indicate exponential fits to the model results.

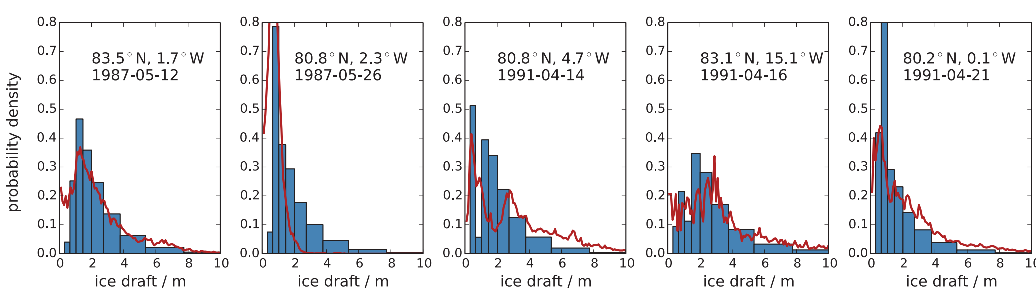

Figure 5. Example of variability in ITDs on small local scales. Plotted are ITDs from 50km submarine track segments (red line) with a snapshot from the nearest grid cell (blue bars). All five observations are taken in Fram Strait in spring (S5).

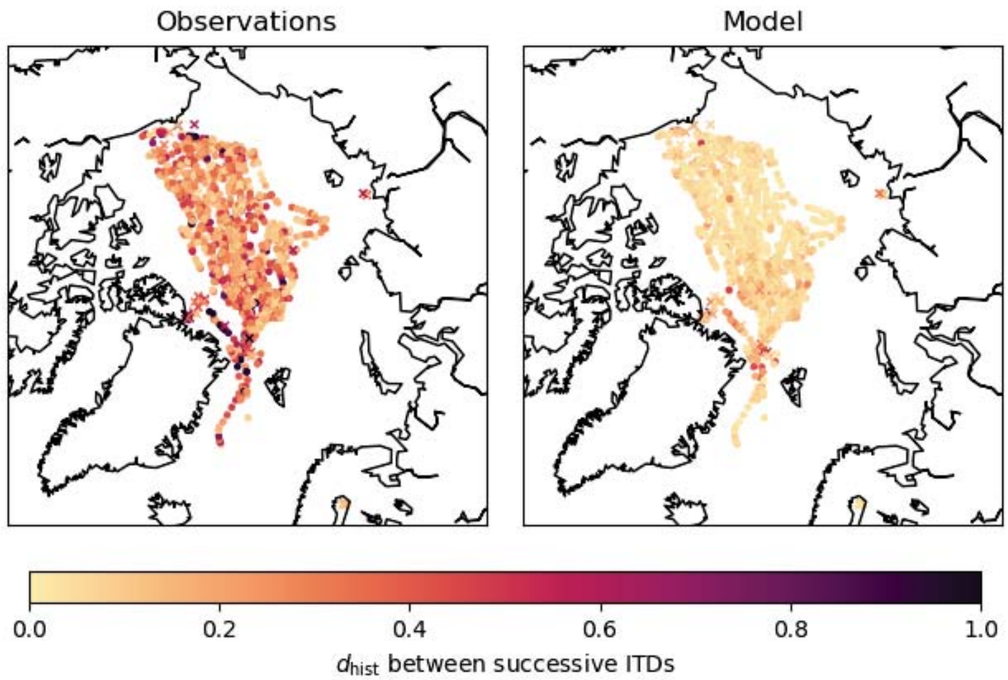

Figure 6. Integrated differences d_{hist} between the cumulative ITDs for successive 50 km track segments (ULS) / successive flights (EM) (left hand side) and between the corresponding model snapshots (right hand side) as a measure of grid-scale variability. Circles mark ULS observations, crosses mark EM observations.

regional mean values because it does not involve any smoothing by averaging. The choice of observations represents the range of locally observed thickness distributions and their simulation in the model. The model distributions follow the main characteristics of the observations. The variability of the local thickness distributions in a given region is generally smaller for the model than for the observations.

We quantify the local variability by calculating the integrated difference d_{hist} between the cumulative thickness distributions for consecutive 50km track segments of ULS campaigns and for consecutive flights in EM sounding campaigns (Figure 6). All successive pairs of observations in the individual campaigns are evaluated except for pairs that are more than 200 km apart. This provides a good coverage of the central half of the Arctic Ocean, although there are more data points in the older ULS data set (1131) than in the more recent EM data set (62). For both data sets, this measure of variability is clearly

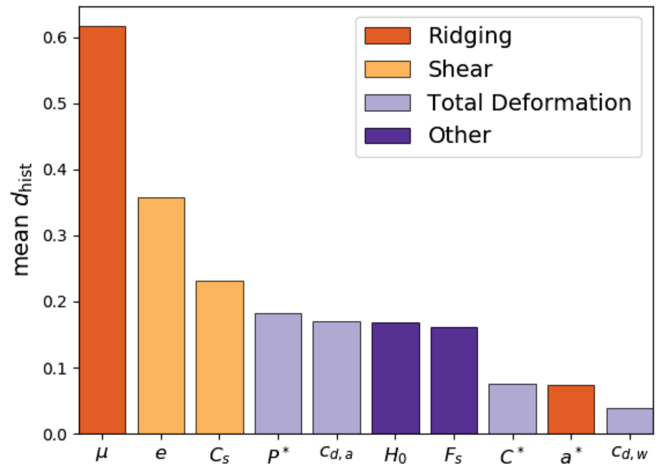

Figure 7. Sensitivity of modeled regional ITDs to each parameter. The difference d_{hist} between the regional ITDs of the positive and negative perturbation simulations is calculated, the mean result is plotted. The color coding refers to different physical mechanisms.

higher for the observations (0.30 m ± 0.26 m for ULS and 0.40 m ± 0.37 m for EM) than for the model (0.06m ± 0.07m for ULS and 0.14 m ± 0.13 m for EM).

3.4 Sensitivity Studies

Sensitivity experiments show the relative impact of ten parameters (Table 2) on the modeled ITDs. The redistribution during ridging (parameter μ) and the deformation in shear (parameters e and C_s) are most important in shaping the modeled ITDs. Figure 7 summarizes the sensitivity of the regional ITDs to the full set of parameters.

Adjusting the ridging parameterization, especially the redistribution of thicknesses during ridging (μ), leads to the largest changes in the modeled ITD. Note that adjusting the participation function (parameter a^*) leaves the ITDs nearly unchanged. The sensitivity of the ITDs to both e and C_s is still larger than the sensitivity to P^* or $c_{d,a}$. This is an interesting result because the ice strength P^* and the atmospheric drag coefficient $c_{d,a}$ are among the most commonly used parameters for tuning sea ice models towards large-scale observations [*Nguyen et al.*, 2011]. Our results suggest that they are not the first choice for tuning regional ITDs.

4 Discussion

The model with ITD parameterization simulates regional and seasonal differences in ITDs accurately compared to corresponding observations. To our best knowledge, we show with unprecedented detail that an ITD model not only simulates average ice conditions in one region accurately [e.g. *Dupont et al.*, 2015; *Herzfeld et al.*, 2015], but also successfully simulates very different regional and seasonal ITDs with the same configuration and parameter set. The model tends to produce distributions with a thin peak and an exponentially decaying tail of thicker, ridged ice. On the one hand, this leads to small model-observation misfits for conditions of relatively uniform first-year ice, for example, in the Beaufort Sea. On the other hand, bi-modal distributions with multiple ice types, which are common for example in Fram Strait, are poorly represented.

The modeled ITDs do not change very much over 15 years. We calculated a reduction of mean ice and snow thickness from the observations for a similar time span. However, the ULS data are collected before 1997 and generally overestimate mean ice thickness, while the EM data are collected after 2001 and underestimate mean ice thickness, so that the computed difference in mean thickness probably overestimates the actual changes. *Rothrock et al.* [2008] found the Arctic wide mean sea ice draft to have decreased by 0.54 m over 15 years. The underlying data set was far more comprehensive than ours, which allowed to reduce the bias between ULS and EM data. Still, the reduction of 0.54 m is bigger than even the largest ice thickness reduction in our model.

Our simulated grid-cell ITDs reproduce mean conditions, but underestimate the variability between points that are in close proximity. Previous comparisons of ITDs from single grid cells of an Arctic model [*Hibler*, 1980] or of results of single-column ITD models [*Schramm et al.*, 1997; *Bellchamber-Amundrud et al.*, 2002] to the few then available point-wise observations agree with ours in that sea ice simulations with the ITD parameterization are consistent with observed Arctic ITDs and that the parameterization can be tuned to a specific set of observations. But with the currently available data, we can go further to show that the parameterization simulates ITDs in single grid cells that are very similar to the regional mean states, but underestimate the observed variability between neighboring grid cells.

In the following subsections, we discuss two possible sources of differences between model and observations: the sea ice thermodynamics and the sea ice deformation. A detailed evaluation of modeled ITDs can help to discriminate between these processes as a source of error.

4.1 Thermodynamics

Modeled ITDs are not very different between different decades. Both the Arctic-wide decadal trends in sea ice extent and in sea ice volume are low in the model when compared to satellite observations or other, well-validated model results. In the following we speculate that the simple 0-layer thermodynamics of our model is one reason for the low interdecadal variability.

The 0-layer thermodynamics were derived to provide a simple, cost-efficient, and easy to implement way to calculate thermodynamic fluxes through the ice [*Semtner*, 1976] at the cost of reduced physical realism. With this parameterization, sea ice does not possess any internal heat capacity, so that the ice warms instantaneously and melting processes start as soon as the air temperatures rise above the freezing point in spring. The consequence is a phase error of approximately one month and a tendency to overestimate the seasonal sea ice thickness cycle [*Semtner*, 1984]. These systematic biases can be reduced by adjusting other sea ice parameters, especially albedo and sea ice conductivity to adjust ice growth and melt rates, and ridging parameters to arrive at realistic mean sea ice thicknesses for unrealistic growth rates [*Semtner*, 1984].

In spite of the simple thermodynamics, the seasonal cycle in the model configuration of this study matches the reference data very closely for pan-Arctic integral properties. This is so because most parameter values in this study are based on results from previous model optimizations against large sets of different observations [*Nguyen et al.*, 2011; *Ungermann et al.*, 2017] to reduce the typical biases associated with 0-layer thermodynamics. It is reasonable to think that this parameter optimization led to some sort of overfitting: We assume that the choice of parameters does not describe the underlying physical processes faithfully, but leads to a nonlinear combination of effects that produces the good match to observations. Such an overfitting to the limited time span of reliable observations may explain why both climate sensitivities and long-term changes in the ITDs are underestimated in the model.

We find that our model underestimates mean ice thickness to a smaller degree than modal ice thickness. The modal thickness in Arctic ITDs is a standard diagnostic in evaluations of high-resolution ice thickness observations [e.g. *Haas and Howell*, 2015], because it describes mostly undeformed, thermodynamically grown ice. In contrast, sea ice models are often evaluated against mean sea ice thickness [e.g. *Chevallier et al.*, 2016; *Stroeve et al.*, 2014]. Again, tuning the models towards this target can introduce compensating biases in the thermodynamics and the ridging schemes: in most regional ITDs our model simulates a mode that is too thin compared to observations; this mode is compensated by a heavier tail leading to a mean thickness that hides the model deficit. This indicates weaker thermodynamic ice growth and compensating ridge distributions in the model compared to observations. *Herzfeld et al.* [2015] simulated ice draft distributions with characteristics in the Fram Strait that are similar to ours (Section 3) even though they use a model with much more sophisticated thermodynamics. From this we speculate that compensating biases exist also in more sophisticated models, and that an evaluation of the modal thickness can help to identify some of them.

In passing we note that the reported effects of the 0-layer thermodynamics, especially the rapid onset and high melt rates in fall, may explain why there are no bi-modal ITDs in the model. In every spring and summer, ice melts too rapidly, so that ice surviving the melting season is not sufficiently thick to produce a distinct, thicker second mode, or to create a first mode as thick as in the observations. In spite of the inaccurate physics on the small scale that lead to missing modes in the ITDs, we do not observe the unrealistically strong seasonal cycle for ice thickness that is expected for 0-layer thermodynamics. A more detailed examination of these processes on a local scale is beyond the scope of this study.

4.2 Sea Ice Deformation

The redistribution of ice thickness due to ridging depends directly on the deformation field (equation 6). A realistic model representation of sea ice deformation in shear [*Bouchat and Tremblay*, 2017; *Wang et al.*, 2016; *Kwok and Cunningham*, 2016] and the scaling of sea ice deformation on small scales [*Weiss and Dansereau*, 2017; *Oikkonen et al.*, 2017; *Spreen et al.*, 2017; *Hutter et al.*, 2018] are current research topics. In this section we show that both deformation in shear and the localization of deformation are inherently connected to the simulation of ITDs.

We find that the exponential decay of the tail of the simulated distributions is indicative of an appropriate model of the physics of ridging. The exponentially decreasing tail of thick ice is a common feature of observed Arctic ice thickness distributions [*Wadhams and Davy*, 1986]. Similar tails are simulated with different ITD models with constant redistribution [*Bellchamber-Amundrud et al.*, 2002; *Godlovitch et al.*, 2012] suggesting that the exponential tails are not created by the explicitly exponential redistribution functions used in this study. Instead, their results suggest that the appropriate physical mechanisms included in the ITD parameterization are not sensitive to the details of the redistribution function. But note that the inaccurately modeled slopes of the exponential distributions (Figure 4) in combination with the difficulty of tuning model coefficients to minimize competing biases (see section 4.1) indicate that one set of parameters in the redistribution functions that has been tuned to fit mean thickness does not necessarily lead to realistic ridging behavior in all forcing situations. *Kubat et al.* [2010] tune redistribution schemes to reproduce individual deformation events accurately. Choosing a comparable target for parameter optimization may reduce possible biases that are introduced to the ridging parameterization when tuning it towards mean ice thickness. However, as long as, for example, the consolidation of multi-year ridges is not explicitly included in the model and ridge properties are solely determined by the initial ridging process, adjusting the ridging parameters (such as μ in this study) can change the ridge geometries to be more in line with first-year or multi-year ice [*Lipscomb et al.*, 2007]. Especially with the strong reduction of the multi-year ice fraction over the last decades [*Polyakov et al.*, 2012], this may limit the ability of current redistribution schemes to reproduce shifts in the ITDs.

The sensitivity studies emphasize how important deformation properties in shear are for sea ice models. Both shear parameters e and C_s are used in many current sea ice models with their default values. These values of $e = 2$ [*Hibler*, 1979] and $C_s = 0.5$ [*Flato and Hibler*, 1995] are not very well constrained by observations. For example, decreasing the value of e can improve the representation of different Arctic-wide sea ice features [*Miller et al.*, 2005; *Lemieux et al.*, 2016; *Bouchat and Tremblay*, 2017; *Ungermann et al.*, 2017]. Furthermore, a recent study analyzed deformation fields and thickness changes from coinciding satellite observations and suggested that the majority of mechanical ice thickness redistribution is caused by shear instead of convergence [*Kwok and Cunningham*, 2016]. Our results support the notion that deformation in shear is a key factor in shaping different ITDs in the Arctic and that stronger ridging caused by shear (i.e., a larger value of C_s = 0.85) is required to improve the model simulations with respect to observed ITDs. At the same time, we note that with a redistribution scheme tuned towards direct observations of deformation events as in *Kubat et al.* [2010] it should be possible to constrain uncertain shear parameters such as e with the increasing number of regional ITD observations.

Finally, low- and medium-resolution models with a viscous-plastic rheology and smooth and slow atmospheric forcing are known to produce unrealistically smooth deformation fields [*Girard et al.*, 2009]. This agrees with our observations of low grid-scale variability in the ITDs: Since the deformation fields with our grid resolution of 36km have only very few sharp features, the deformation history of neighboring grid cells should be very similar. Increasing the resolution of similar VP models allows to reach a realistic degree of localization of deformation, even though the intermittency continues to be underestimated [*Hutter et al.*, 2018]. We note that in our comparison of 1D observations to 2D model results, the 2D results are already smoother by representing an average of 2 dimensions. Still, from future high-resolution simulations of model configurations with a dynamic ITD we may learn if the appropriate localization of deformation is more important than tuning shear deformation parameters of ITDs or vice versa. New rheologies may simulate the observed intermittency of deformation more realistically than the VP-rheology. Comparing different rheologies in high-resolution simulations may then provide insight into whether localization of deformation is more important than its intermittency in the simulation of ITDs. In addition, comparing different rheologies in high-resolution simulations may inform about the role of grid-scale ITDs in generating intermittency of deformation.

5 Conclusions

From a comparison of modeled ITDs against observations from different regions, seasons and decades in the Arctic, we draw the following conclusions: With the currently used form of ITD parameterizations one can accurately reproduce many but not all ice thickness distributions under different forcing situations in the Arctic in the same simulation. Observed regional and seasonal variations in ITDs in the Arctic are, to a large degree, reproduced both in regional averages and snapshots from single grid cells. Individual regional ITDs have been modeled successfully before, but here we show a general agreement in a pan-Arctic sea ice - ocean model. Decadal variations in ITDs, however, are lower than observed

The modeled ITDs depend on the overall drift and thickness patterns and hence on parameters that are not directly related to the ITD parameterization. In some cases the model does not capture the mode and tail of observed ice thickness distributions. There are many potential reasons for this and we have tried to attribute some of these issues to simplified thermodynamics and inaccurate deformation fields. The attribution is not complete and it is difficult to disentangle all different process that are involved.

With the many new high resolution thickness data, we presented the shape of ITDs, and especially their modal thickness, as new, and easy to implement model diagnostics. The modal thickness is a key parameter in evaluating observations, and we suggest that it should also be used in evaluating model results. The modal thickness diagnostic allows to separate more clearly thermodynamic and dynamic effects in thickness patterns, and can thereby reduce potentially compensating biases in these two parameterizations.

Variability in ITDs between adjacent grid points is low in the model. The parameterization should be local by design, yet the simulated ITDs in individual grid cells react mostly to regional conditions. We identify different possible causes, with smooth deformation fields in medium resolution VP models as the most probable one. Future studies with dynamic ITD parameterizations in high resolution models can identify if improved localization of deformation will improve grid cell ITDs or if low intermittency in deformation is a limiting factor.

Acknowledgments

We would like to thank Martin Vancoppenolle and Fred Dupont for their helpful reviews on this paper. Observational data are taken from [*Lindsay and Schweiger*, 2013] (ULS) and [*Haas et al.*, 2006, 2008, 2010] (EM). Model data will be made available at PANGAEA upon acceptance of the paper. This project was supported by the Deutsche Forschungsgemeinschaft (DFG) through the International Research Training Group IRTG 1904 ArcTrain.

References

Arctic Council (2009), Arctic Marine Shipping Assessment 2009 Report, *Tech. rep.*

Bellchamber-Amundrud, T., H. Melling, and G. Ingram (2002), Modelling the Evolution of Draft Distribution in the Sea Ice Pack of the Beaufort Sea, in *Ice in the Environment: Proceedings of the 16th IAHR International Symposium on Ice*, December.

Bitz, C. M., M. M. Holland, A. J. Weaver, and M. Eby (2001), Simulating the ice-thickness distribution in a coupled climate model, *Journal of Geophysical Research*, *106*, 2441, doi:10.1029/1999JC000113.

Bouchat, A., and B. Tremblay (2017), Using sea-ice deformation fields to constrain the mechanical strength parameters of geophysical sea ice, *Journal of Geophysical Research: Oceans*, *122*(7), 5802–5825, doi:10.1002/2017JC013020.

Chevallier, M., G. C. Smith, F. Dupont, J.-F. Lemieux, G. Forget, Y. Fujii, F. Hernandez, R. Msadek, K. A. Peterson, A. Storto, T. Toyoda, M. Valdivieso, G. Vernieres, H. Zuo, M. Balmaseda, Y.-S. Chang, N. Ferry, G. Garric, K. Haines, S. Keeley, R. M. Kovach, T. Kuragano, S. Masina, Y. Tang, H. Tsujino, and X. Wang (2016), Intercomparison of the Arctic sea ice cover in global oceanâĂŞsea ice reanalyses from the ORA-IP project, *Climate Dynamics*, *SI*, doi:10.1007/s00382-016-2985-y.

Coon, M. D., G. Maykut, R. S. Pritchard, D. A. Rothrock, and A. S. Thorndike (1974), Modeling the Pack Ice as an Elastic-Plastic Material, *AIDJEX Bulletin*, *24*, 1–106.

Dupont, F., S. Higginson, R. Bourdallé-Badie, Y. Lu, F. Roy, G. C. Smith, J.-F. Lemieux, G. Garric, and F. Davidson (2015), A high-resolution ocean and sea-ice modelling system for the Arctic and North Atlantic oceans, *Geoscientific Model Development*, *8*(5), 1577–1594, doi:10.5194/gmd-8-1577-2015.

EUMETSAT Ocean and Sea Ice Satellite Application Facility (2011), Global sea ice concentration reprocessing dataset 1978-2009 (v1.1), [Online]. Norwegian and Danish Meteorological Institutes. Available from http://osisaf.met.no.

Flato, G. M., and W. D. Hibler (1995), Ridging and strength in modeling the thickness distribution of Arctic sea ice, *Journal of Geophysical Research*, *100*(C9), 18,611–18,626.

Flocco, D., and D. L. Feltham (2007), A continuum model of melt pond evolution on Arctic sea ice, *Journal of Geophysical Research*, *112*(C8), doi:10.1029/2006JC003836.

Girard, L., J. Weiss, J. M. Molines, B. Barnier, and S. Bouillon (2009), Evaluation of high-resolution sea ice models on the basis of statistical and scaling properties of Arctic sea ice drift and deformation, *Journal of Geophysical Research: Oceans*, *114*(8), 1–15, doi:10.1029/2008JC005182.

Godlovitch, D., A. Monahan, and G. Flato (2012), An idealised stochastic model of sea ice thickness dynamics, *Cold Regions Science and Technology*, *78*, 14–30, doi: 10.1016/j.coldregions.2012.02.006.

Haas, C., and S. E. L. Howell (2015), Ice thickness in the Northwest Passage, *Geophysical Research Letters*, *42*(18), 7673–7680, doi:10.1002/2015GL065704.

Haas, C., S. Hendricks, and M. Doble (2006), Comparison of the sea ice thickness distribution in the Lincoln Sea and adjacent Arctic Ocean in 2004 and 2005, *Annals of Glaciology*, *44*, 247–252.

Haas, C., A. Pfaffling, S. Hendricks, L. Rabenstein, J. L. Etienne, and I. Rigor (2008), Reduced ice thickness in Arctic Transpolar Drift favors rapid ice retreat, *Geophysical Research Letters*, *35*(17), 1–5, doi:10.1029/2008GL034457.

Haas, C., S. Hendricks, H. Eicken, and A. Herber (2010), Synoptic airborne thickness surveys reveal state of Arctic sea ice cover, *Geophysical Research Letters*, *37*(9), 1–5, doi: 10.1029/2010GL042652.

Herzfeld, U. C., E. C. Hunke, B. W. McDonald, and B. F. Wallin (2015), Sea ice deformation in Fram Strait – Comparison of CICE simulations with analysis and classification of airborne remote-sensing data, *Cold Regions Science and Technology*, *117*, 19–33, doi: 10.1016/j.coldregions.2015.05.001.

Hibler, W. D. (1979), A Dynamic Thermodynamic Sea Ice Model, *Journal of Physical Oceanography*, *9*(4), 815–846, doi:10.1175/1520-0485(1979)009<0815:ADTSIM>2.0.CO;2.

Hibler, W. D. (1980), Modeling a Variable Thickness Sea Ice Cover, *Monthly Weather Review*, *108*(12), 1943–1973.

Holland, M. M., C. M. Bitz, E. C. Hunke, W. H. Lipscomb, and J. L. Schramm (2006), Influence of the sea ice thickness distribution on polar climate in CCSM3, *Journal of Climate*, *19*(11), 2398–2414, doi:10.1175/JCLI3751.1.

Hunke, E. C., W. H. Lipscomb, and A. K. Turner (2010), Sea-ice models for climate study: retrospective and new directions, *Journal of Glaciology*, *56*(200), 1162–1172, doi:10.3189/002214311796406095.

Hutter, N., M. Losch, and D. Menemenlis (2018), Scaling Properties of Arctic Sea Ice Deformation in a High-Resolution Viscous-Plastic Sea Ice Model and in Satellite Observations, *Journal of Geophysical Research: Oceans*, *123*(1), 672–687, doi: 10.1002/2017JC013119.

Johnston, M. E., and C. Haas (2011), Validating Helicpter-based EM (HEM) Thicknesses Over Very Thick Multi-Year Ice, in *Proceedings of the 21st International Conference on Port and Ocean Engineering under Arctic Conditions (POAC '11)*, pp. 1–11, International Conference on Port and Ocean Engineering under Arctic Conditions, Montréal, Canada.

Kimura, N., A. Nishimura, Y. Tanaka, and H. Yamaguchi (2013), Influence of winter sea-ice motion on summer ice cover in the Arctic, *Polar Research*, *32*, 1–8, doi: 10.3402/polar.v32i0.20193.

Komuro, Y., and T. Suzuki (2013), Impact of subgrid-scale ice thickness distribution on heat flux on and through sea ice, *Ocean Modelling*, *71*, 13–25, doi: 10.1016/j.ocemod.2012.08.004.

Kubat, I., M. Sayed, S. B. Savage, and T. Carrieres (2010), Numerical simulations of ice thickness redistribution in the Gulf of St. Lawrence, *Cold Regions Science and Technology*, *60*(1), 15–28, doi:10.1016/j.coldregions.2009.07.003.

Kwok, R., and G. F. Cunningham (2008), ICESat over Arctic sea ice: Estimation of snow depth and ice thickness, *Journal of Geophysical Research*, *113*(C8), C08,010, doi: 10.1029/2008JC004753.

Kwok, R., and G. F. Cunningham (2016), Contributions of growth and deformation to monthly variability in sea ice thickness north of the coasts of Greenland and the Canadian Arctic Archipelago, *Geophysical Research Letters*, *43*(15), 8097–8105, doi: 10.1002/2016GL069333.

Lavergne, T., S. Eastwood, Z. Teffah, H. Schyberg, and L.-A. Breivik (2010), Sea ice motion from low-resolution satellite sensors: An alternative method and its validation in the Arctic, *Journal of Geophysical Research*, *115*(C10), C10,032, doi: 10.1029/2009JC005958.

Lemieux, J.-F., C. Beaudoin, F. Dupont, F. Roy, G. C. Smith, A. Shlyaeva, M. Buehner, A. Caya, J. Chen, T. Carrieres, L. Pogson, P. Derepentigny, A. Plante, P. Pestieau, P. Pellerin, H. Ritchie, G. Garric, and N. Ferry (2016), The Regional Ice Prediction System (RIPS): Verification of forecast sea ice concentration, *Quarterly Journal of the Royal Meteorological Society*, *142*(695), 632–643, doi:10.1002/qj.2526.

Lindsay, R. (2003), Changes in the modeled ice thickness distribution near the Surface Heat Budget of the Arctic Ocean (SHEBA) drifting ice camp, *Journal of Geophysical Research*, *108*(C6), doi:10.1029/2001JC000805.

Lindsay, R., and A. J. Schweiger (2013, updated 2017), Unified Sea Ice Thickness Climate Data Record, 1947 onward, Version 1, doi:http://dx.doi.org/10.7265/N5D50JXV.

Lipscomb, W. H., E. C. Hunke, W. Maslowski, and J. Jakacki (2007), Ridging, strength, and stability in high-resolution sea ice models, *Journal of Geophysical Research: Oceans*, *112*, 1–18, doi:10.1029/2005JC003355.

Losch, M., D. Menemenlis, J. M. Campin, P. Heimbach, and C. Hill (2010), On the formulation of sea-ice models. Part 1: Effects of different solver implementations and parameterizations, *Ocean Modelling*, *33*(1-2), 129–144, doi:10.1016/j.ocemod.2009.12.008.

Marshall, J., A. Adcroft, C. Hill, L. Perelman, and C. Heisey (1997), A finite-volume, ncompressible Navier Stokes model for studies of the ocean on parallel computers, *Journal of Geophysical Research*, *102*(C3), 5753–5766, doi:10.1029/96JC02775.

Massonnet, F., T. Fichefet, H. Goosse, M. Vancoppenolle, P. Mathiot, and C. König Beatty (2011), On the influence of model physics on simulations of Arctic and Antarctic sea ice, *The Cryosphere*, *5*(3), 687–699, doi:10.5194/tc-5-687-2011.

Maykut, G. A. (1978), Energy exchange over young sea ice in the central Arctic, *Journal of Geophysical Research*, *83*(C7), 3646, doi:10.1029/JC083iC07p03646.

McPhee, M. (1975), Ice-Momentum Transfer for the AIDJEX Ice Model, *AIDJEX Bulletin*, *29*, 93–112.

Menemenlis, D., J-M. Campin, P. Heimbach, C. Hill, T. Lee, A. Nguyen, M. Schodlok, and H. Zhang (2008), ECCO2: High resolution global ocean and sea ice data synthesis, *Mercator Ocean Quarterly Newsletter*, *31*(October), 13–21.

Miller, P. A., S. W. Laxon, and D. L. Feltham (2005), Improving the spatial distribution of modeled Arctic sea ice thickness, *Geophysical Research Letters*, *32*(18), doi: 10.1029/2005GL023622.

MITgcm Group (2016), MITgcm Manual.

Nguyen, A. T., D. Menemenlis, and R. Kwok (2011), Arctic ice-ocean simulation with optimized model parameters: Approach and assessment, *Journal of Geophysical Research: Oceans*, *116*(4), 1–18, doi:10.1029/2010JC006573.

Oikkonen, A., J. Haapala, M. Lensu, J. Karvonen, and P. Itkin (2017), Small-scale sea ice deformation during N-ICE2015: From compact pack ice to marginal ice zone, *Journal of Geophysical Research: Oceans*, *122*(6), 5105–5120, doi:10.1002/2016JC012387.

Overland, J. E., M. Wang, J. E. Walsh, and J. C. Stroeve (2013), Future Arctic climate changes : Adaptation and mitigation time scales, *Earth's Future*, *2*, 68–74, doi:

10.1002/2013EF000162.Received.

Pfaffling, A., C. Haas, and J. E. Reid (2007), Direct helicopter EM âĂŤ Sea-ice thickness inversion assessed with synthetic and field data, *Geophysics*, *72*(4), F127–F137, doi: 10.1190/1.2732551.

Polyakov, I. V., J. E. Walsh, and R. Kwok (2012), Recent changes of Arctic multiyear sea ice coverage and the likely causes, *Bulletin of the American Meteorological Society*, *93*(2), 145–151, doi:10.1175/BAMS-D-11-00070.1.

Reid, J. E., A. Pfaffling, and J. Vrbancich (2006), Airborne electromagnetic footprints in 1D earths, *Geophysics*, *71*(2), 63–72, doi:10.1190/1.2187756.

Rothrock, D. A., and M. Wensnahan (2007), The accuracy of sea ice drafts measured from U.S. Navy submarines, *Journal of Atmospheric and Oceanic Technology*, *24*(11), 1936–1949, doi:10.1175/JTECH2097.1.

Rothrock, D. A., D. B. Percival, and M. Wensnahan (2008), The decline in arctic sea-ice thickness: Separating the spatial, annual, and interannual variability in a quarter century of submarine data, *Journal of Geophysical Research: Oceans*, *113*(5), 1–9, doi: 10.1029/2007JC004252.

Roy, F., M. Chevallier, G. C. Smith, F. Dupont, G. Garric, J.-F. Lemieux, Y. Lu, and F. Davidson (2015), Arctic sea ice and freshwater sensitivity to the treatment of the atmosphere-ice-ocean surface layer, *Journal of Geophysical Research: Oceans*, *120*, 4392–4417, doi:10.1002/2014JC010677.

Rubner, Y., C. Tomasi, and L. J. Guibas (2000), The Earth Mover's Distance as a Metric for Image Retrieval, *International Journal of Computer Vision*, *40*(2), 99–121, doi: 10.1023/A:1026543900054.

Saha, S., S. Moorthi, H. L. Pan, X. Wu, J. Wang, S. Nadiga, P. Tripp, R. Kistler, J. Woollen, D. Behringer, H. Liu, D. Stokes, R. Grumbine, G. Gayno, J. Wang, Y. T. Hou, H. Y. Chuang, H. M. H. Juang, J. Sela, M. Iredell, R. Treadon, D. Kleist, P. Van Delst, D. Keyser, J. Derber, M. Ek, J. Meng, H. Wei, R. Yang, S. Lord, H. Van Den Dool, A. Kumar, W. Wang, C. Long, M. Chelliah, Y. Xue, B. Huang, J. K. Schemm, W. Ebisuzaki, R. Lin, P. Xie, M. Chen, S. Zhou, W. Higgins, C. Z. Zou, Q. Liu, Y. Chen, Y. Han, L. Cucurull, R. W. Reynolds, G. Rutledge, and M. Goldberg (2010), The NCEP climate forecast system reanalysis, *Bulletin of the American Meteorological Society*, *91*(August), 1015–1057, doi:10.1175/2010BAMS3001.1.

Schramm, J. L., M. M. Holland, and J. A. Curry (1997), The effects of snowfall on a snow-ice-thickness distribution, *Annals of Glaciology*, *25*(25), 287–291.

Schweiger, A., R. Lindsay, J. Zhang, M. Steele, H. Stern, and R. Kwok (2011), Uncertainty in modeled Arctic sea ice volume, *Journal of Geophysical Research*, *116*(September), doi:10.1029/2011JC007084.

Semtner, A. J. (1984), On modelling the seasonal thermodynamic cycle of sea ice in studies of climatic change, *Climatic Change*, *6*(1), 27–37, doi:10.1007/BF00141666.

Semtner, A. J. J. (1976), A model for the thermodynamic growth of sea ice in numerical investigations of climate, *Journal of Physical Oceanography*, *6*, 379–389.

Spreen, G., R. Kwok, D. Menemenlis, and A. T. Nguyen (2017), Sea-ice deformation in a coupled oceanâĂŞ-sea-ice model and in satellite remote sensing data, *The Cryosphere*, *11*(4), 1553–1573, doi:10.5194/tc-11-1553-2017.

Stroeve, J. C., A. P. Barrett, M. C. Serreze, and A. Schweiger (2014), Using records from submarine, aircraft and satellite to evaluate climate model simulations of Arctic sea ice thickness, *The Cryosphere*, *8*, 2179–2212, doi:10.5194/tcd-8-2179-2014.

Sumata, H., T. Lavergne, F. Girard-Ardhuin, N. Kimura, M. A. Tschudi, F. Kauker, M. Karcher, and R. Gerdes (2014), An intercomparison of Arctic ice drift products to deduce uncertainty estimates, *Journal of Geophysical Research: Oceans*, *119*, doi:10.1002/2013JC009724.

Sumata, H., R. Kwok, R. Gerdes, F. Kauker, and M. Karcher (2015), Uncertainty of Arctic summer ice drift assessed by high-resolution SAR data, *Journal of Geophysical Research: Oceans*, *120*, 5285–5301, doi:10.1002/2014JC010632.

Thorndike, A. S., D. A. Rothrock, G. A. Maykut, and R. Colony (1975), The Thickness Distribution of Sea Ice, *Journal of Geophysical Research*, *80*(33), 4501–4513, doi:10.1029/JC080i033p04501.

Tsamados, M., D. L. Feltham, D. Schroeder, D. Flocco, S. L. Farrell, N. Kurtz, S. W. Laxon, and S. Bacon (2014), Impact of Variable Atmospheric and Oceanic Form Drag on Simulations of Arctic Sea Ice, *Journal of Physical Oceanography*, *44*(5), 1329–1353, doi:10.1175/JPO-D-13-0215.1.

Ungermann, M., L. B. Tremblay, T. Martin, and M. Losch (2017), Impact of the ice strength formulation on the performance of a sea ice thickness distribution model in the Arctic, *Journal of Geophysical Research: Oceans*, *122*, 2017–2033, doi:10.1002/2016JC012128.

Wadhams, P., and T. Davy (1986), On the spacing and draft distributions for pressure ridge keels, *Journal of Geophysical Research*, *91*(C9), 10,697, doi: 10.1029/JC091iC09p10697.

Wang, Q., S. Danilov, T. Jung, L. Kaleschke, and A. Wernecke (2016), Sea ice leads in the Arctic Ocean: Model assessment, interannual variability and trends, *Geophysical Research Letters*, *43*(13), 7019–7027, doi:10.1002/2016GL068696.

Warren, S. G., I. G. Rigor, N. Untersteiner, V. F. Radionov, N. N. Bryazgin, Y. I. Aleksandrov, and R. Colony (1999), Snow depth on Arctic sea ice, *Journal of Climate*, *12*, 1814–1829, doi:10.1175/1520-0442(1999)012<1814:SDOASI>2.0.CO;2.

Weiss, J., and V. Dansereau (2017), Linking scales in sea ice mechanics, *Philosophical Transactions of the Royal Society A: Mathematical, Physical and Engineering Sciences*, *375*(2086), 20150,352, doi:10.1098/rsta.2015.0352.

Windnagel, A., M. Savoie, and W. Meier (2016), Sea Ice Index Version 2 Analysis, *Tech. rep.*, National Snow and Ice Data Center, Boulder CO, USA.